Available online at www.sciencedirect.com
SCIENCE DIRECT
Polymer 47 (2006) 6149–6155
polymer
www.elsevier.com/locate/polymer

Morphology of PI–PEO block copolymers for lithium batteries

Chenchen Xue [a], Mary Ann B. Meador [b,*], Lei Zhu [c], Jason J. Ge [a], Stephen Z.D. Cheng [a], Sirina Putthanarat [d], R.K. Eby [a,*], Ameesh Khalfan [e], George D. Bennett [e], Steve G. Greenbaum [e]

[a] *Maurice Morton Institute of Polymer Science, The University of Akron, Akron, OH 44325, USA*
[b] *NASA Glenn Research Center, Materials Division, Mail Stop 49-3, 21000 Brookpark Road, Cleveland, OH 44135, USA*
[c] *Institute of Materials Science and Department of Chemical Engineering, The University of Connecticut, Storrs, CT 06269, USA*
[d] *University of Dayton, UDRI 300, College Park, Dayton, OH 45469, USA*
[e] *Physics Department, Hunter College of CUNY, New York, NY 10021, USA*

Received 6 March 2006; received in revised form 26 May 2006; accepted 3 June 2006
Available online 7 July 2006

Abstract

Polyimide (PI)–polyethylene oxide (PEO) block copolymers have a wide variety of applications in microelectronics, since PI–PEO films exhibit a high degree of thermal and chemical stability. The polymers consist of short, rigid rod T-shaped PI segments, alternating with flexible, PEO coil segments. The highly incompatible PI rods and PEO coils should phase-separate, especially in the presence of lithium ions used as electrolytes for lithium polymer batteries. The rigid rod phase provides a high degree of dimensional stability. In this paper, we provide evidence by DSC that the self-assembled ordered structure of the PI–PEO molecules is formed from concentrated solution rather than the bulk state. Tapping mode AFM and X-ray diffraction are applied to observe the nanodomains in the phase separation of the PI and PEO before and after doping with lithium ions. In addition, we report evidence of the ion transport primary mechanism, in the amorphous phase of the lithium salt-doped PI–PEO block copolymers' multinuclear NMR linewidth, spin-lattice relaxation time, and pulsed field gradient diffusion measurements.

Keywords: Lithium batteries; Solid polymer electrolytes; Morphology

1. Introduction

Rod-coil molecules are a novel type of block copolymer with unique microstructure due to their ability to self-assemble to various ordered morphologies on a nanometer length scale [1]. These molecules, comprised of two homopolymers joined end to end, microphase separate into ordered, periodic arrays of spheres and cylinders in the bulk state and/or solution [2,3]. Recent applications of block copolymers include use as solid polymer electrolytes for lithium batteries. After Wright's discovery of ionic conductivity in alkali metal salt complexes of poly(ethylene oxide) [4], these polymers were proposed as electrolytes for batteries by Armand et al. [5] since they combine the advantages of solid-state electrochemistry with the ease of processing inherent to plastic materials. The poly(ethylene oxide) structure is the basis for many electrolytes currently under study because of its ability to solvate lithium ions. However, long chains of poly(ethylene oxide) tend to crystallize and slow ion mobility at temperatures below about 80 °C, unless the crystalline units are aligned [6]. Various approaches to prevent this crystallization are currently under study [7], including plasticizers [8], hyperbranched polymers [9], and the use of nanoparticle additives [10]. One of the more intriguing approaches involves the use of copolymers that phase-separate into nanodomains. For example, Soo et al. [11] have demonstrated this concept with a system in which one of the domains is a poly(methyl methacrylate) with ethylene oxide side chains and the other is a siloxane. Though both domains consist of polymers that are well above their glass transition temperature (T_g) at room temperature, the interface imparts solid behavior upon films fabricated from the blocks and room temperature ionic conductivities are quite high. Molecular dynamic simulations

* Corresponding authors. Tel. +1 216 433 3221; fax: +1 216 977 7132.
E-mail addresses: maryann.meador@nasa.gov (M.A.B. Meador), reby@uakron.edu (R.K. Eby).

0032-3861/$ - see front matter © 2006 Elsevier Ltd. All rights reserved.
doi:10.1016/j.polymer.2006.06.024

suggest that the lithium ions are complexed with PEO through approximately five ether oxygens of a PEO chain.

Okamoto et al. have reported block copolymers consisting of rod-coil structures [12,13]. The short, rigid rod segment and flexible, polyalkylene oxide coil segment are phase-separated into two major domains, which increase the selectivity for CO_2/N_2 gas separation. They have found that the linear polyimide rods show the best gas separation properties due to the phase separation.

Recently, Meador and coworkers have reported a similar class of branched polyimides (PI)–polyethylene oxide (PEO) polymers and examined their behavior as possible electrolytes for lithium polymer batteries [14,15]. Whereas the coil phase allows conduction of lithium ions better at room temperature than high molecular weight PEO, the more rigid polyimide rod phase with a very high T_g, provides improved physical properties over other phase-separated polymer electrolytes.

In this paper, we give a detailed study of the morphologies of the branched PI–PEO films. The self-assembled ordered structure of the PI–PEO molecules, consisting of short, rigid rod T-shaped PI segments, alternating with flexible, PEO coil segments is formed from concentrated solution. Morphology of the phase separation is monitored by small angle X-ray scattering (SAXS) and Atomic Force Microscopy (AFM). Direct evidence of the ion transport primary mechanism along the amorphous phase of the lithium salt-doped PI–PEO block copolymers shown is provided by ^{7}Li and ^{19}F NMR relaxation and transport measurements.

2. Experimental

A fully branched PI–PEO with a formulated molecular weight of 60 000, $n = 10.72$ g/mol as shown in Scheme 1 was prepared as previously described with and without lithium doping at a Li:O ≈ 0.05 (the molar ratio of lithium salt over oxygen of ethylene oxide units) [15]. The ionic conductivity of the lithium containing polymer has been previously reported as 2.45×10^{-5} S/cm at room temperature [15]. The samples were stored in vacuum before characterization and analysis.

Differential scanning calorimetry (DSC, Perkin–Elmer PYRIS Diamond) experiments were carried out to study the isothermal crystallization and melting behaviors of un-doped PI–PEO. The DSC instrument was calibrated with *p*-nitrotoluene, naphthalene, and indium standards. Isothermal crystallization was conducted by quenching the samples from 120 °C to the preset T_c. The fully crystallized samples were then heated to 80 °C at a rate of 5 °C/min. The endothermic peak temperature was taken as the melting temperature (T_m).

A Rigaku 18-kW rotating-anode generator (Cu K) equipped with an image plate and a hot stage was used to obtain high-quality fiber patterns after 30 min to 1 h of exposure times. The diffraction 2θ positions and widths observed on the powder and fiber patterns were calibrated with silicon crystals with known 2θ diffractions and crystallite sizes when $2\theta > 15°$ and calibrated with silver behenate when $2\theta < 15°$.

Transmission electron microscopy (TEM) studies were conducted using a JEOL 1200EX II at an accelerating voltage of 120 kV. Thin slices of block copolymer for TEM observation were obtained using a Reicher Ultracut S (Leica) cryomicrotome at −120 °C. The thin film thickness was around 100 nm. Phase contrast was obtained by staining in vapor of a 3% RuO_4 water solution for 20 min. The PEO phase was stained, since it was more easily oxidized than the PI phase.

Atomic Force Microscopy (AFM, Digital Instrument Nanoscope IIIa) was used to examine the surface topology of the thin film treated as described before [14,15]. A 100 μm scanner was selected and a tapping mode was used to obtain both height and phase images. The scanning frequency was controlled within 0.2–0.5 Hz for the low magnification images. The data were collected with a 512 × 512 pixel per image resolution.

The NMR measurements were performed on a Chemagnetics CMX-300 spectrometer in which the Larmor frequencies of ^{7}Li and ^{19}F are 116.9 and 283.2 MHz, respectively. Variable temperature spectral linewidths, spin-lattice relaxation times (T_1) and self-diffusion coefficients were investigated. Measurements were made using 0.5–1.0 g samples which were loaded and packed into flame-sealed 5-mm Pyrex tubes in a very low humidity (<1 ppm) dry-box (VAC). Self-diffusion coefficients were obtained by the NMR Pulse Gradient Spin-Echo technique [16], which uses the Hahn spin-echo pulse sequence ($\pi/2-\tau-\pi$), with typical $\pi/2$ pulse width of 5 μs for ^{7}Li and 11 μs for ^{19}F, on a Nalorac Z-Spec gradient probe. For a diffusing spin in the presence of a magnetic field, the application of square-shaped magnetic field gradient pulses of magnitude g results in the attenuation of the echo amplitude A, represented by: $A(G) = \exp[-\gamma^2 G^2 D\delta 2(\Delta - (\delta/3))]$, where D is the self-diffusion coefficient for a range of gradient strengths G from 0.2 to 1.2 T/m, γ is the nuclear gyromagnetic ratio, Δ is the time interval between two gradient pulses and δ is the duration of the single gradient pulse. For the polymer electrolytes

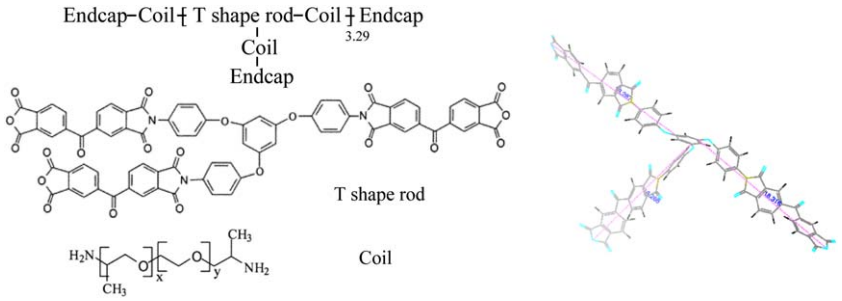

Scheme 1. PI–PEO block copolymer structure and T-shaped imide rod conformation of computer simulation.

investigated, the experimental parameters Δ and δ, given in ms, ranged from 45 to 100 and 15 to 25, respectively, for ^{7}Li, and from 25 to 35 and 4 to 5, respectively, for ^{19}F. Uncertainties in self-diffusion measurements are about 3–5%. NMR spectra were obtained by transforming the resulting free induction decay (FID) of a single $\pi/2$ pulse sequence or a solid echo ($\pi/2_x-\tau-\pi/2_y$) pulse sequence. Spin-lattice relaxation times, T_1, were obtained by inversion recovery. Uncertainties in T_1 determinations were about 3%. The sample was allowed to equilibrate for 20–25 min between temperature changes.

3. Results and discussion

3.1. Crystallinity and phase separation of un-doped PI–PEO

The solution self-assembled phase behavior of the un-doped PI–PEO has been examined with SAXS at room temperature as shown in Fig. 1. A diffraction scattering halo with a d spacing of 13 nm is observed, indicating that a microphase separation occurred when the PI–PEO polymer was cast from solution in *N*-methylpyrrolidinone (NMP). It is known that the phase behavior of a bulk block copolymer actually depends on three physical events, which compete with each other or override one another in forming the final phase and crystalline morphologies in amorphous–crystalline block copolymers. These events are the microphase separation of the block copolymers at T_{ODT} (order–disorder transition), the crystallization of the crystallizable blocks at T_c^c, and the vitrification of the amorphous blocks at T_g^a. To form a microphase separated structure, T_{ODT} should be larger than T_g^a. Since TMA experimental results have shown that the T_g^a of PI is above 200 °C and the T_{ODT} is in the range of 80–110°, it can safely be said that the microphase separation of this PI–PEO material is occurring in solution rather than in the bulk state. Direct evidence is provided by AFM phase (right) and height (left) images in Fig. 2. In the phase image, some lamellar structures stack on top of the others, while some align edge to edge. The lamellar thickness measured from the height image is in the range from 11 to 15 nm, which is in agreement with the SAXS experiment result. AFM experiments were also performed below 10 °C (Fig. 3). In the phase image, some PEO crystals are formed between (region A in Fig. 3) and in (region B in Fig. 3) the lamellas. In region A, the lamellas are edge on and expanded by PEO crystals with a dimension of 16 nm. In region B, actually in one lamella, the PEO crystallized in the lamella with dimension of 16 nm. To understand how the molecules self-assemble into this ordered structure, the molecular conformation of the crystallizable PEO coil and the amorphous PI rod must be studied.

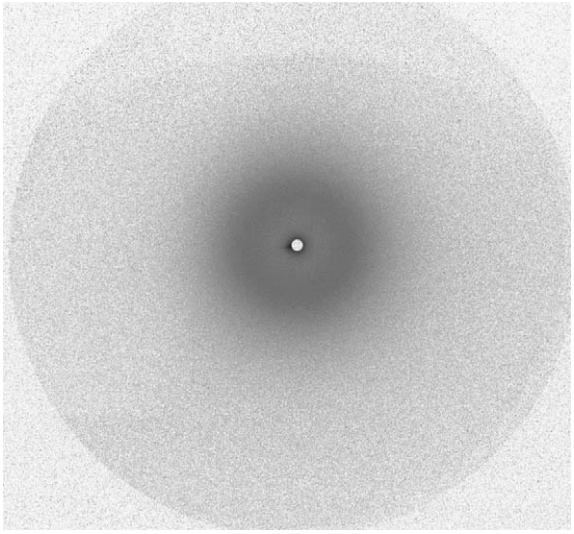

Fig. 1. High-resolution synchrotron SAXS pattern.

To investigate the possible effects of the molecular architecture of PEO on this confined environment, a wide angle X-ray diffraction (WAXD) experiment has been carried out at 5 °C. Fig. 4 demonstrates the typical WAXD pattern. The diffraction rings at $2\theta = 19°$ come from the (120) plane, and the ring around $2\theta = 23°$ is actually multiple diffraction rings with contributions from diffraction of several crystal

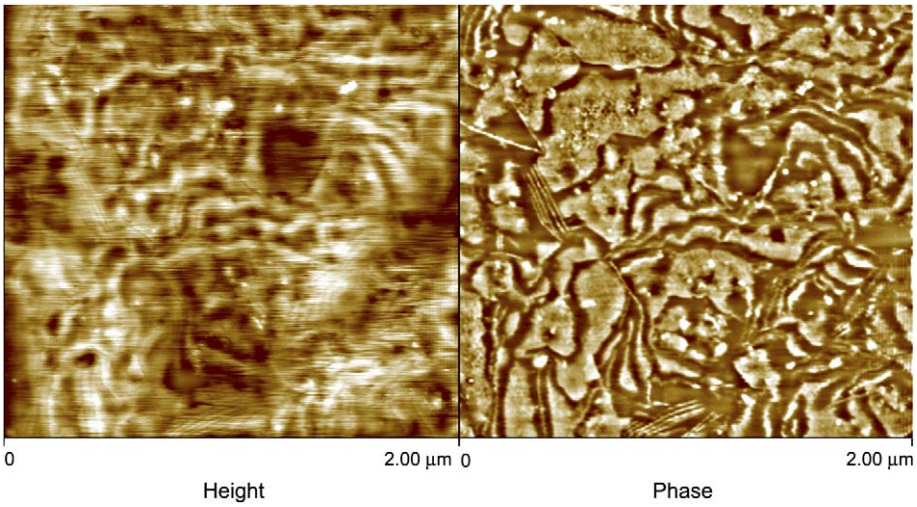

Fig. 2. AFM height (left) and phase (right) images of PI–PEO block copolymer at room temperature.

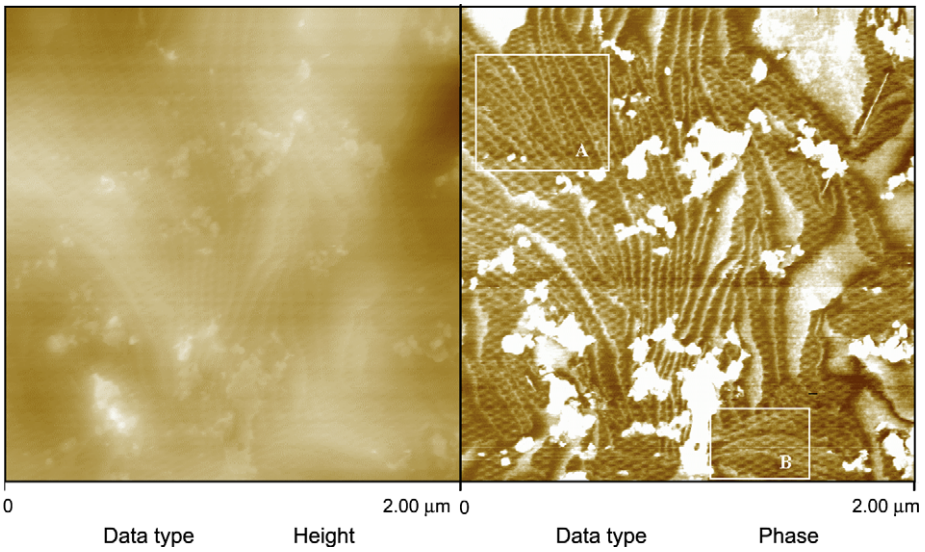

Fig. 3. AFM height (left) and phase (right) images below 10 °C.

planes. The linear PEO can be fitted into a monoclinic crystal structure. The unit cell parameters are $a = 0.805$ nm, $b = 1.304$ nm, $c = 1.948$ nm and $\beta = 125.4°$ [17]. The repeating unit in a single chain shows a succession of *trans*, *trans*, *gauche* (*ttg*) conformations. The *ttg* conformation exhibits a (7/2) helix with D_7 symmetry. D_7 indicates a dihedral molecular symmetry and the subscript denotes a sevenfold screw axis parallel to the molecular axis. Since the period of the *c*-axis includes seven repeating units, each repeating unit possesses a length of 0.278 nm in the crystalline portion. The average chain length, L, is given by the following equation: $L = 0.278 \times M_n/44$, where 44 is the molecular weight of one PEO repeat unit. In our case, the extended PEO chain length is about 12.6 nm with a molecular weight of 2000.

The computer simulation provides the T-shaped rod length parameter shown in Scheme 1. The length of the rod in the main chain is 3.7 nm and the length of the rod in the side chain is 1.8 nm. By combining the molecular conformation and the AFM experimental results, a probable microphase separation model has been provided (Fig. 5). In this model, the T blocks represent the T-shaped rigid imide rods and the lines represent the extend PEO chains. Fig. 5a is the side view of the lamellas, which consist of the main chain polymers. The side chains with rod and PEO crystals will separate the lamellae. This model depends on the inter-molecular phase separation between PEO in side chains and imide rods in the main chain. The top view of the lamellas is shown in Fig. 5b. The intra-molecular phase separation between PEO crystals and imide rods will direct the main chains to form this kind of lamella.

To further examine the lamellar formation of the PEO in the confined space, isothermal melt crystallization was studied by cooling the melt rapidly to a designated crystallization temperature (T_c). As the T_c increases, the crystallization exotherms shift to higher temperatures and become broad. The Avrami equation [18], which assumes that the relative degree of crystallinity (X_t) develops with time t, was used to analyze

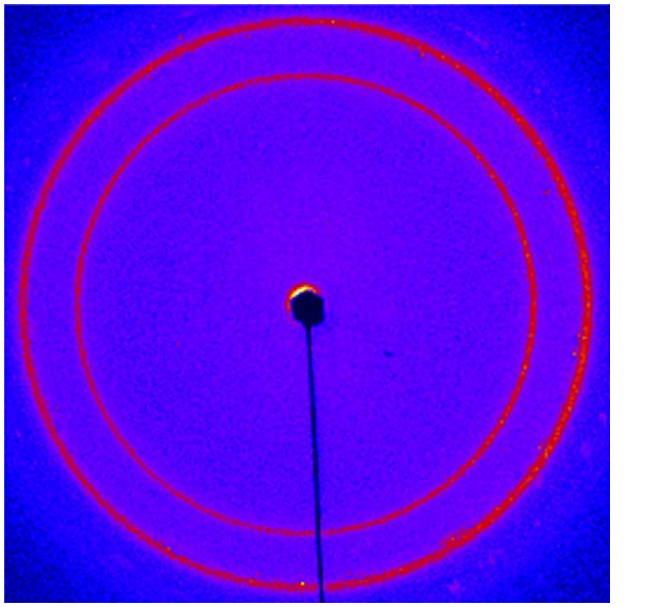

Fig. 4. 2D WAXD pattern. (The first reflection ring is (120) reflection. The second ring includes the (−130), (032), (−212), (112), (−124) and (004) reflections.)

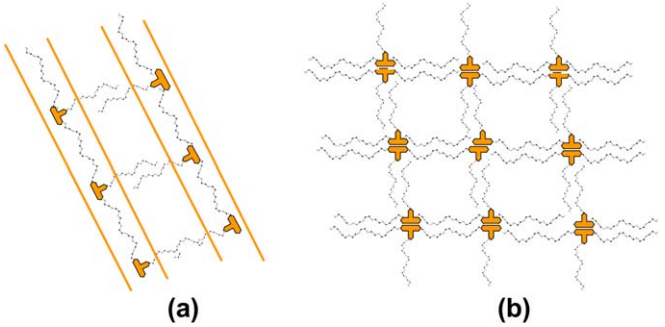

Fig. 5. Most probable model (a) lamellar side view and (b) lamellar top view.

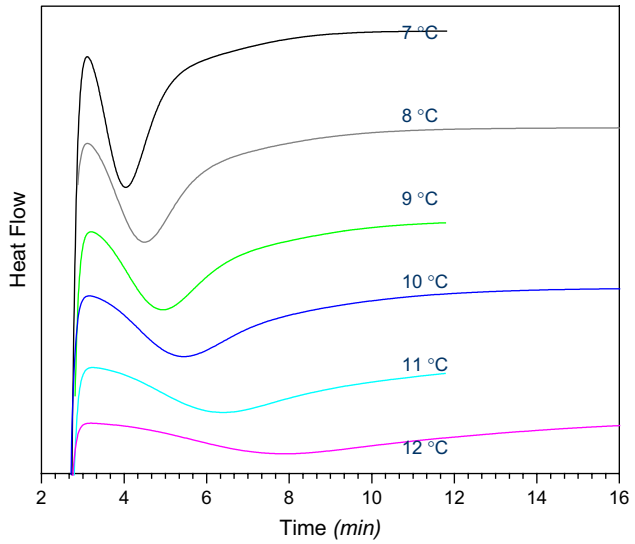

Fig. 6. DSC curves of heat flow vs. time during isothermal crystallization. (The numbers for the lines represent the crystallization temperatures.)

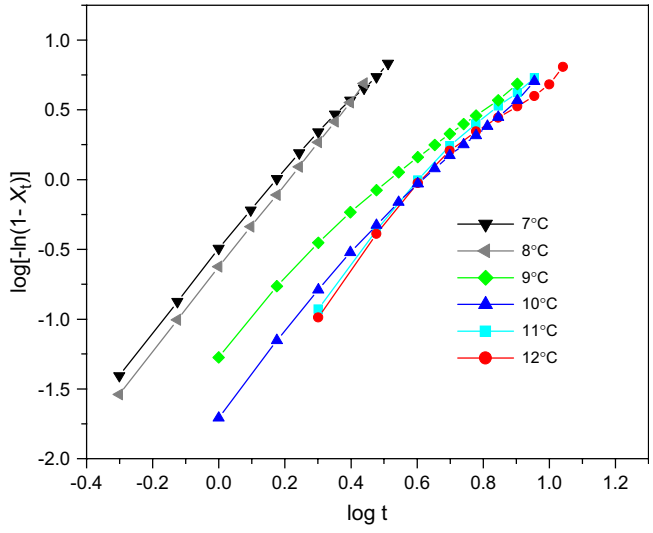

Fig. 7. Plots of $\log[-\ln(1-X_t)]$ vs. $\log(t)$ for isothermal crystallization. (The numbers for the lines represent the crystallization temperatures.)

the isothermal crystallization process of PEO. The development of relative crystallization with time for isothermal crystallization from the melt is shown in Fig. 6. The relative amount of crystallinity that develops at a definite time decreases with increasing crystallization temperature T_c. The degree of crystallinity of the PEO block can be also measured from wide angle X-ray diffraction by resolving the total intensity curve into three curves representing diffracted X-ray intensities from amorphous material and (120) crystalline planes. The well-known double logarithmic plots $\log[-\ln(1-X_t)]$ vs. $\log(t)$ are shown in Fig. 7. Each curve shows an initial linear portion, subsequently tending to level off. This deviation was considered to be due to the secondary impingement in the later stage [19]. The Avrami parameter n for PEO crystals determined from the initial linear portion in Fig. 7 represents the PEO crystallization mechanism. The n values at different crystallization temperatures are from 2.85 to 2.88 °C, which indicate that the PEO is crystallized in a lamellar behavior.

3.2. Lithium doped PI–PEO

As previously reported, the PI–PEO doped with Li at a Li:O ≈ 0.05 (the molar ratio of lithium salt over oxygen of ethylene oxide units) has no crystalline transition as evidenced by DSC and the T_g increases by 8–10 °C over that of the un-doped film (−56 °C) [15]. Morphology of the doped polymer was investigated by AFM tapping model. In the right phase image of Fig. 8, we observe no crystalline lamellae as in the un-doped PI–PEO copolymer in Fig. 2. Only phase separation is observed. This is also seen in a TEM of the sample stained using RuO_4 after cutting samples of a thickness of about 50 nm as shown in Fig. 9. Since PEO-rich phases are more easily stained, they appear darker than the PI-rich phase. There is no obvious ordered structure in the micrograph. Hence, both AFM and TEM results provide further evidence that the lithium doped block copolymer is in an amorphous state.

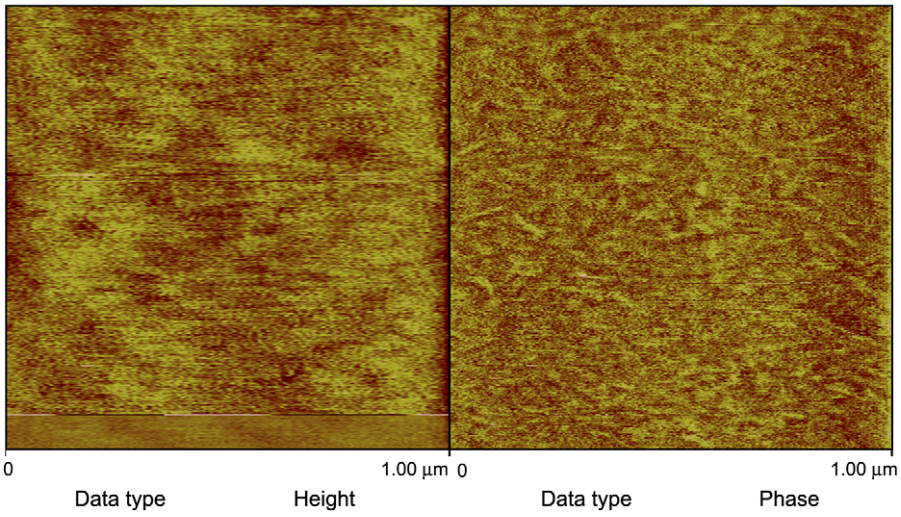

Fig. 8. AFM height (left) and phase (right) images of lithium doped PI–PEO block copolymer at room temperature.

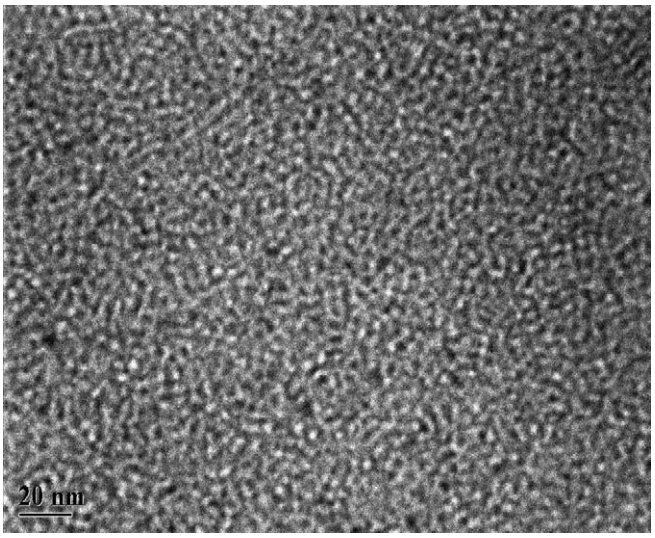

Fig. 9. TEM observation of the lithium doped PI–PEO block copolymer after RuO_4 staining.

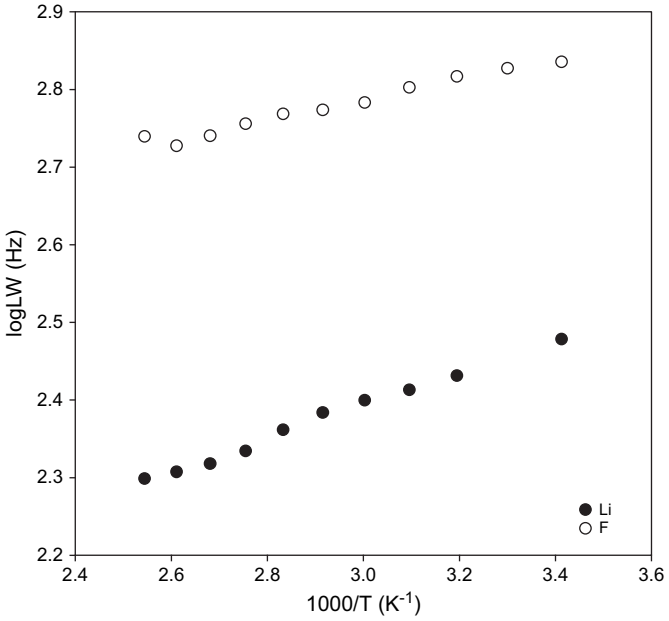

Fig. 10. Arrhenius plot of ^{7}Li and ^{19}F NMR linewidths in lithium doped PI–PEO block copolymer.

3.3. Transport studies

Early studies of PEO-based electrolytes suggested a crystalline phase transport mechanism involving ionic conduction through the PEO helices [5], however, the vast majority of subsequent investigations have shown that the ion transport occurs primarily in the amorphous phase [20]. On the other hand, under certain conditions for comparable compositions, the crystalline phase cation transport can exceed that of the amorphous phase [21], and the crystalline phase transport can be significantly augmented when the polymer is aligned through mechanical [22] or magnetic means [6]. However, in randomly oriented systems (as in the present case), it can be assumed that the amorphous phase transport mechanism is the dominant one.

Arrhenius plots of NMR linewidth, spin-lattice relaxation (T_1), and self-diffusion coefficients (D), corresponding to both cations and anions (^{7}Li and ^{19}F, respectively), are displayed in Figs. 10–12, respectively. The cation- and anion-associated linewidths (Fig. 10) exhibit similar activation energies, suggesting a common factor that influences their dynamical behavior, i.e. segmental motion of the PEO phase. Spin-lattice relaxation is most sensitive to motional processes near the reciprocal angular NMR frequency, in fact more rapid than those probed by the linewidth measurements. The T_1 results in Fig. 11 revealed different behaviors for the cations and anions, partly due to the higher ^{19}F resonance frequency as compared to ^{7}Li, but also attributed to other factors. In particular, the ^{7}Li T_1 exhibits a minimum near 345 K, whereas the ^{19}F T_1 minimum is less apparent due to the limited temperature range at the lower end, but possibly occurring at around 295 K. Efficient spin-lattice relaxation could in fact be achieved through rotation of the CF_3 group on the anion, which is independent of translational motion.

Finally, the cation and anion diffusion results in Fig. 12 indicate similar temperature dependencies, again suggesting that both ionic mobilities are linked to the common mechanism of polymer segmental motion in the amorphous phase. The anion diffusion is significantly higher than the cation diffusion despite its larger size, consistent with behavior observed for the vast majority of polyether-based polymer electrolytes, and again, a consequence of amorphous phase transport [9,16,20]. In oriented polymer electrolyte systems involving crystalline phase transport, cation conductivities tend to be somewhat higher [21,22].

4. Conclusions

In summary, the structural analysis via SAXS and AFM combined with the molecular conformation determined by

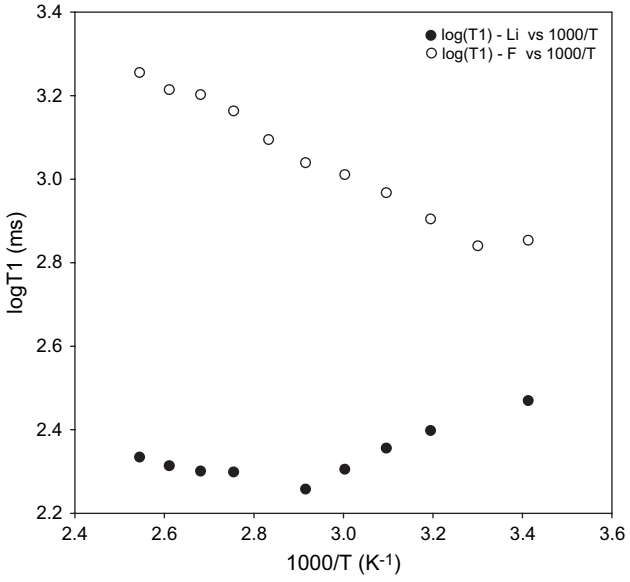

Fig. 11. Arrhenius plot of ^{7}Li and ^{19}F NMR spin-lattice relaxation times in lithium doped PI–PEO block copolymer.

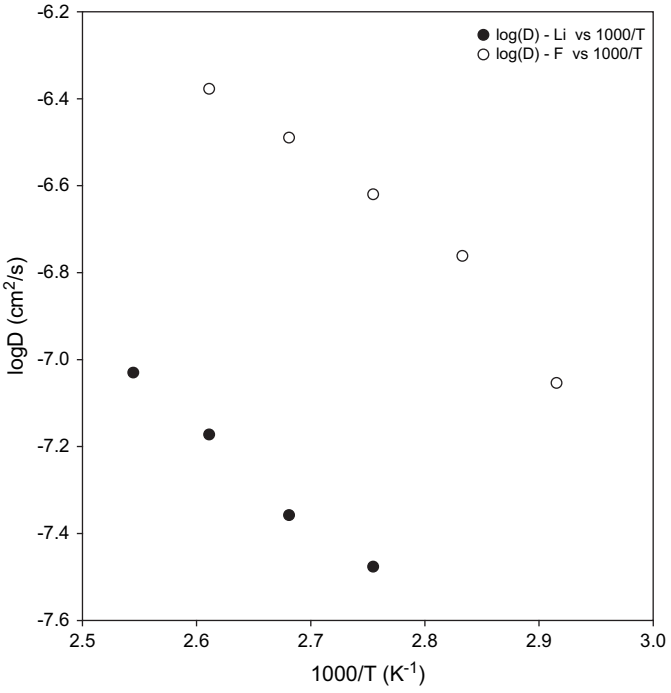

Fig. 12. Arrhenius plot of ^{7}Li and ^{19}F NMR self-diffusion coefficients in lithium doped PI–PEO block copolymer.

WAXD and DSC experiments have provided experimental evidence to determine the inter- and intra-molecular phase separation of the rod-coil block copolymer from the solution state. It is clear that the nano-confined environment formed by the rods will control PEO melting and crystallization behavior, and most likely helps to maintain an amorphous state for lithium ion conduction in the doped polymers.

Acknowledgements

We thank the Advanced Battery Program of the NASA Glenn Research Center for support of this project. Financial support to Hunter College from the MBRS-RISE (NIH) program and an RCMI (NIH) Infrastructure grant (#RR-03037) are gratefully acknowledged.

References

[1] Bates FS, Fredrickson GH. Annu Rev Phys Chem 1990;41:525.
[2] Zhu L, Cheng SZD, Calhoun BH, Ge Q, Quirk RP, Thomas EL, et al. J Am Chem Soc 2000;122:5957.
[3] Park C, Rosa CDe, Fetters LJ, Thomas EL. Macromolecules 2000; 33:7931.
[4] Fenton DE, Parker JM, Wright PV. Polymer 1973;14:589.
[5] Armand MB, Chabagno JM, Duclot M. Fast ion transport in solids. In: Vashishta P, Mundy JN, Shenoy GK, editors. New York: North Holland; 1979. p. 131.
[6] Golodnitskyz D, Livshits E, Kovarsky R, Peled E, Chung SH, Suarez S, et al. Electrochem Solid-State Lett 2004;7:A412–5.
[7] Wright PV. MRS Bull 2002;27:597–602.
[8] Kim YT, Smotkin ES. Solid State Ionics 2002;149:29–37.
[9] Nishimoto A, Agehara K, Furuya N, Watanabe T, Watanabe M. Macromolecules 1999;32:1541–8.
[10] Croce F, Persi L, Scrosati B, Serraino-Fiory F, Plichta E, Hendrickson MA. Electrochim Acta 2001;46:2457.
[11] Soo PP, Huang B, Sadoway DR, Mayes AM. J Electrochem Soc 1999; 146:32.
[12] Yoshino M, Ito K, Kita H, Okamoto K. J Polym Sci B Polym Phys 2000;38:1707–15.
[13] Okamoto K, Fujii M, Okamyo S, Suzuki H, Tanaka K, Kita H. Macromolecules 1995;28:6950–8.
[14] Initial screening of other rod and coil combinations was reported in Meador MAB, Cubon VA, Schieman DA, Bennett W. 11th International meeting on lithium batteries. In: Meeting abstracts, 153. Pennington, NJ: The Electrochemical Society; June 23–28, 2002.
[15] Meador MAB, Cubon VA, Scheiman DA, Bennett WR. Chem Mater 2003;15:3018.
[16] Stejskal EO, Tanner JE. J Chem Phys 1965;42:288–92.
[17] Takahashi Y, Tadokoro H. Macromolecules 1973;6:672.
[18] Avrami M. J Chem Phys 1939;7:1103.
[19] Lee Y, Porter RS. Macromolecules 1988;21:2770.
[20] Ratner M, Johanson P, Shriver DF. MRS Bull 2000;25:31–8.
[21] Gadgourova Z, Andreev Y, Tunstall D, Bruce P. Nature (London) 2001; 412:520–3.
[22] Golodnitsky D, Peled E, Livshits E, Ulus A, Barkay Z, Lapides I, et al. J Phys Chem A 2001;105:10098–106.